

Proceedings of the ASME 2022
International Design Engineering Technical Conferences and
Computers and Information in Engineering Conference
IDETC-CIE2022
August 14-17, 2022, St. Louis, Missouri

DETC2022-91109

ANALYSIS OF A NONLINEAR LOCALLY RESONANT METAMATERIAL WITH RESISTANCE-INDUCTANCE SHUNT

Arun Malla, Mohammad Bukhari, Oumar Barry*

Department of Mechanical Engineering Virginia Polytechnic Institute and State University Blacksburg, Virginia 24061

ABSTRACT

The study of metamaterials for simultaneous vibration control and energy harvesting is a subject with considerable recent interest. This paper investigates a weakly nonlinear metamaterial with electromechanical local resonators coupled to a resistance-inductance shunt circuit, a system with no previous examination in the literature. The nonlinear band structure of the system is presented to demonstrate the effect of an inductor in the shunt circuit, including the influence on softening and hardening nonlinearity effects. The system is then excited by a transient wavepacket and simulated numerically to further explore the features of nonlinear wave propagation in the proposed structure for multiple inductance values. Particularly, the system's voltage response is studied through spatial profiles to observe the effects of shunt inductance, nonlinearity, and any potential interaction between the two. Focus is given to the potential for vibration control and energy harvesting by this metamaterial, including comparisons to previously investigated similar systems with resistance-only shunt circuit. For certain parameters including high electromechanical coupling, the band structure of this system is shown to include three mode branches instead of the twomode band structure observed in the absence of shunted inductor. Strong vibration attenuation is observed in the frequency range around the central mode branch. The effects of the inductor on wave propagation and harvested voltage are also shown.

1 Introduction

Metamaterials are artificially engineered structures that possess properties not found in naturally occurring materials [1]. The unusual features of metamaterials make them beneficial for numerous applications including vibration and noise control, energy harvesting, non-destructive testing, and acoustic rectifiers.

Metamaterials consist of many unit cells arranged in periodic or aperiodic patterns. It has been observed that periodic structures prevent waves from propagating through the structure at certain frequency ranges, known as band gaps [2–4]. Because these band gaps are constrained by the unit cell dimensions, the application of basic metamaterials was limited to large structures [1]. To expand the use of metamaterials to smaller components, Liu et al. introduced local resonators, showing that locally resonant metamaterials are able to control vibrations at wavelengths much smaller than the lattice constant [5]. Local resonators are also capable of widening the original band gap. Further manipulation of the system's band structure can also be achieved by introducing multiple resonators [6,7].

Band gaps can also be introduced by the incorporation of piezoelectric materials and shunt circuits. Piezoelectric materials have long been utilized in both active and passive methods for vibration control [8–11], and more recently have been incorporated into metamaterials [12–14]. By including piezoelectric elements in a metamaterial, the mechanical system dynamics can be coupled to an easily modifiable shunt circuit, enabling convenient adjustment of the metamaterial's overall properties. Incorporating piezoelectric materials and shunt circuits enables techniques such as the use of negative capacitance [15] or resonant shunt circuits

^{*}Corresponding Author (Email: obarry@vt.edu)

cuits [16] to control vibrations and create or broaden band gaps. In addition, shunt circuits also offer an avenue for simultaneous energy harvesting. An important parameter in any work involving piezoelectric materials is the system's electromechanical coupling factor. This parameter is dependent on the design and material properties of the piezoelectric component [17]. Though this piezoelectric coupling coefficient is usually on the order of 10^{-10} for engineering applications [18], signifying weak electromechanical coupling, some features may only be apparent in the case of strong electromechanical coupling.

These two methods have also been utilized in concert, with researchers investigating metamaterials with both local resonators and shunt circuits. For instance, Sugino et al. studied a locally resonant material coupled to a shunt with piezoelectric elements [17]. Bukhari also examined a system with local resonators, shunt circuits, and weakly nonlinear springs [19]. However, none of the aforementioned works examined a nonlinear metamaterial with an inductor coupled to the energy harvester. The focus of the current study is to determine the effects of that added inductor on the band structure and nonlinear response of the system. This paper investigates a nonlinear acoustic metamaterial with local resonators coupled to resistance-inductance shunt circuits. This metamaterial is modeled through a nonlinear system of governing equations, and excited by a transient wave packet. Numerical methods are applied to investigate the effect of shunt circuit parameters and nonlinearity on wave propagation and energy harvesting. Specifically, the spatial profile of the voltage response is studied for multiple shunt inductance values in order to explore interesting nonlinear wave propagation phenomena. The primary focus of this work is to study effects of shunt inductance on system response, as well as any potential interaction with nonlinearity, focusing on the resultant applications for simultaneous vibration control and energy harvesting.

2 Mathematical Modeling of the System

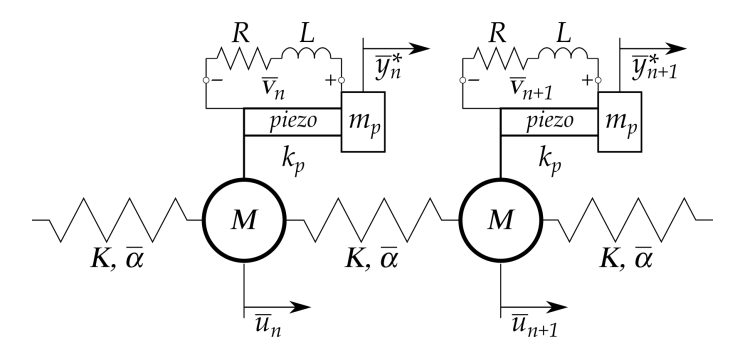


FIGURE 1: Schematic of nonlinear metamaterial with electromechanical resonators.

This work focuses on a metamaterial consisting of a chain of cells connected by nonlinear springs, depicted in Fig. 1. Each nonlinear spring has linear spring coefficient K and nonlinear spring coefficient $\bar{\alpha}$. Each cell is coupled to a local resonator, with each resonator including a substrate covered by a piezo-electric layer, with total effective mass m_p and effective linear stiffness k_p . The piezoelectric layer is shunted to a resistance-inductance (RL) circuit as shown in Fig. 1. This shunt circuit has voltage difference \bar{v}_n , resistance R, and inductance L. The piezoelectric layer has capacitance C_p and electromechanical (EM) coupling coefficient θ . The absolute displacement of cell n is \bar{u}_n , and the absolute displacement of the attached piezoelectric resonator is \bar{y}_n^* .

Following [19] and [20], the governing equations of a coupled cell, local resonator, and shunt circuit can be written for infinite chain as:

$$M\ddot{u}_{n} + 2K\bar{u}_{n} - K\bar{u}_{n+1} - K\bar{u}_{n-1} + \bar{\alpha}(\bar{u}_{n} - \bar{u}_{n+1})^{3} + \bar{\alpha}(\bar{u}_{n} - \bar{u}_{n-1})^{3} + m_{n}(\ddot{u}_{n} + \ddot{y}_{n}) = 0$$
(1)

$$m_p \ddot{y}_n + k_p \ddot{y}_n - \theta (L\dot{v}_n/R + \bar{v}_n) = -m_p \ddot{u}_n \tag{2}$$

$$LC_{p}\ddot{\mathbf{v}}_{n} + RC_{p}\dot{\mathbf{v}}_{n} + \bar{\mathbf{v}}_{n} + R\theta\dot{\mathbf{y}}_{n} = 0 \tag{3}$$

where $\bar{y}_n = \bar{y}_n^* - \bar{u}_n$ is the relative displacement of piezoelectric local resonator n with respect to cell n.

Eq. (3) can be rewritten as:

$$\frac{1}{\omega_e^2} \ddot{v}_n + RC_p \dot{v}_n + \bar{v}_n + R\theta \dot{y}_n = 0 \tag{4}$$

where $\omega_e = 1/\sqrt{LC_p}$ is the electric resonance frequency.

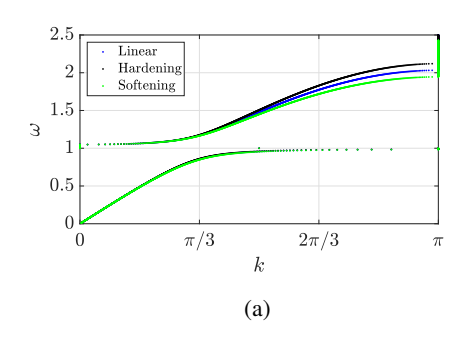
The system of governing equations Eqs. (1), (2), and (4) can be nondimensionalized by substituting nondimensional variables: $u_n = \bar{u}_n/U_0$, $y_n = \bar{y}_n/U_0$, $v_n = \bar{v}_n/V_0$, and nondimensional time $\tau = \omega_n t$, where $\omega_n = \sqrt{K/M}$ is the mechanical natural frequency of the main cell. This results in the system:

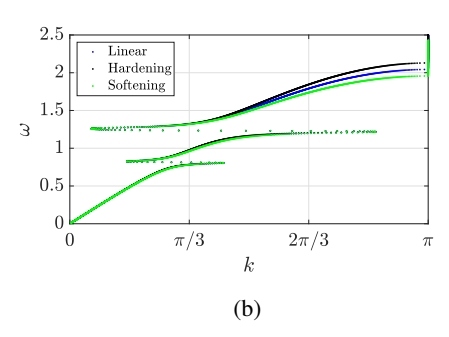
$$\ddot{u}_n + 2u_n - u_{n+1} - u_{n-1} + \alpha (u_n - u_{n+1})^3 + \alpha (u_n - u_{n-1})^3 + \bar{k}\Omega_1^2 (\ddot{u}_n + \ddot{y}_n) = 0$$
(5)

$$\Omega_1^2 \ddot{y}_n + y_n - \alpha_1 (\alpha_3 \dot{v}_n + v_n) = -\Omega_1^2 \ddot{u}_n$$
 (6)

$$\Omega_2^2 \ddot{v}_n + \alpha_2 \dot{v}_n + v_n + \alpha_4 \dot{y}_n = 0 \tag{7}$$

where $\alpha = \bar{\alpha}U_0^2/K$, $\Omega_1 = \omega_n/\omega_p$, $\omega_p^2 = k_p/m_p$, $\bar{k} = k_p/K$, $\alpha_1 = \theta V_0/k_p U_0$, $\alpha_3 = L\omega_n/R$, $\Omega_2 = \omega_n/\omega_e$, $\alpha_2 = RC_p\omega_n$, and $\alpha_4 = R\theta\omega_n U_0/V_0$.





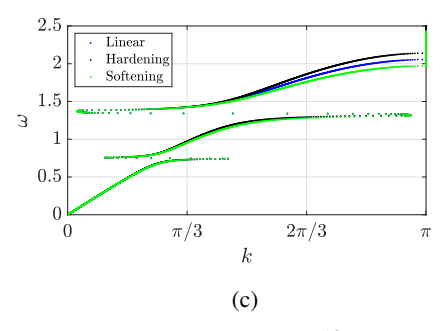


FIGURE 2: Effect of EM coupling and shunt inductance on nonlinear band structure: (a) Weak EM coupling, $\theta = 10^{-10}$ N/V; default shunt inductance $L = L_0$; (b) Strong EM coupling, $\theta = 10^{-1}$ N/V; $L = L_0$; (c) Strong EM coupling, increased shunt inductance $L = 2L_0$.

3 Band Structure Analysis

To derive dispersion relations for the nonlinear system, the perturbation method of multiple scales (MMS) is utilized, following the procedure outlined by Nayfeh in [21]. First we introduce a small dimensionless parameter ε ($\varepsilon \ll 1$) in the governing equations by defining multiple time scales: the fast time scale, $T_0 = \tau$; and the slow time scale, $T_1 = \varepsilon \tau$. The time derivative operators are then perturbed and can be expressed as:

$$\frac{\partial}{\partial \tau} = D_0 + \varepsilon D_1 + O(\varepsilon^2) \tag{8a}$$

$$\frac{\partial^2}{\partial \tau^2} = D_0^2 + 2\varepsilon D_0 D_1 + O(\varepsilon^2) \tag{8b}$$

where $D_n = \partial/\partial T_n$.

Following this, the solution for main cell displacement $u(T_0)$ can be expressed as a power series in powers of ε as

$$u_n(\tau) = u_{n,0}(T_0, T_1) + \varepsilon u_{n,1}(T_0, T_1) + O(\varepsilon^2),$$
 (9)

In addition, the governing equations are converted into a weakly nonlinear form by rescaling the parameter $\alpha = \alpha \varepsilon$. After substituting Eq. (8) into Eqs. (5)-(7), collecting terms of ε^0 and ε^1 yield the linear and nonlinear problems, respectively. For the linear system, the solution $u(T_0)$ can be expressed in polar form as:

$$u_{n,0}(T_0) = Ae^{i(nk - \omega T_0)} + c.c.$$
 (10)

where ω and k are the linear frequency (normalized by ω_n) and wavenumber, respectively; and c.c. denotes the complex conjugate of the preceding term.

Substituting Eq. (10) into the linear system and solving for A provides the linear dispersion relation:

$$-\omega^2 + 2 - 2\cos(k) - \Omega_1^2 \bar{k}\omega^2 (1 + \Gamma_2) = 0$$
 (11)

 Γ_2 is a function of ω^2 and various system parameters:

$$\Gamma_2 = \frac{\Omega_1^2 \omega^2}{1 - \Omega_1^2 \omega^2 + i\alpha_1 \alpha_3 \Gamma_1 \omega - \alpha_1 \Gamma_1}$$
(12)

where Γ_1 is defined as:

$$\Gamma_1 = \frac{i\alpha_4\omega}{1 - \Omega_2^2\omega^2 - i\alpha_2\omega} \tag{13}$$

Solving Eq. (11) reveals six roots for ω in the form of three complex conjugate pairs. Consequently, the linear band structure may have up to three pass bands depending on the system parameters.

The nonlinear solution is derived from the collected ε^1 terms. To solve the nonlinear system, the polar form of A is substituted:

$$A(T_1) = \frac{1}{2}a(T_1)e^{ib(T_1)} \tag{14}$$

Then, separating real and imaginary parts yields the slow flow equations:

$$a' = c_0 a^3 \tag{15}$$

$$b' = c_1 a^2 \tag{16}$$

where ' represents derivative with respect to T_1 . c_0 and c_1 are functions of ω , k, and various system parameters:

The nonlinear frequency of the system is found by applying the correction factor b' to the linear frequency as follows:

$$\omega_{NL} = \omega - \varepsilon b' \tag{17}$$

Using the solutions for linear and nonlinear frequency in Eqs. (11) and (17), the linear and nonlinear band structures of the proposed metamaterial are examined in the form of dispersion curves. For this work, the following parameter values are used: The mass of each main cell is M=0.125 kg, and the mass ratio between each piezeoelectric resonator and main cell is $m_p/M=0.1$. The mechanical and electrical natural frequencies of the resonator, ω_p and ω_e , are tuned to the main cell natural

frequency ω_n such that $\omega_n = \omega_p = \omega_e = 2e5$ rad/s. These values were chosen based on the similar system studied by Abdelmoula et al. in [20]. For these parameters, it can be assumed a' = 0 and thus $b' = c_1 a_0^2$, where $a_0 = a(0)$ is a constant. Nonlinearity is varied by changing the nonlinear parameter $\varepsilon \alpha a_0^2$, with $\varepsilon \alpha a_0^2 = 0$ for the linear chain, 0.06 for nonlinear hardening, and -0.06 for nonlinear softening.

As the focus of this paper is on the effect of shunt inductance, the EM coupling coefficient is set to strong coupling, $\theta = 10^{-1}$ N/V, and shunt resistance is set to $R = 10^3 \Omega$. If the system has weak EM coupling $\theta < 10^{-2} N/V$, its band structure matches the metamaterial with resistance-only shunt studied by Bukhari [19], with two pass bands as shown in Fig. 2(a). In this case, shunt inductance has no significant effect on the band structure. Raising the shunt resistance to $R > 10^3 \Omega$ also results in a two-branch band structure which is not affected by shunt inductance. However, with strong EM coupling and relatively low shunt resistance as described above, the system has a band structure with three pass bands as shown in Fig. 2(b). Pass bands and band gaps can be tuned with shunt inductance and other system parameters. For instance, Fig. 2(b) and (c) show linear and nonlinear dispersion curves for the case of default shunt inductance, $L = L_0 = 0.2212$ H; and the case of doubled shunt inductance, $L = 2L_0$; respectively. The most prominent effect of the large inductance is an increase in the frequency bandwidth of the second mode branch. The effects of nonlinearity remain consistent for both values of L. Nonlinear hardening shifts the dispersion curves up on the frequency axis, while softening shifts them down. The magnitude of the shift is negligible for small wavenumber k (long wavelength limit) as well as low frequencies. Effects of nonlinearity are more pronounced for the third mode branch, especially at larger wavenumbers (short wavelength limit). Due to this, the bandwidth of the third mode increases for hardening chain and decreases for softening chain. In constrast, for the first and second modes, the effects of nonlinearity are minimal at both small and large wavenumbers; thus, the effect of nonlinearity is most significant in the medium wavenumber region. This results in no significant change in the bandwidth of these modes or the adjacent band gaps due to nonlinearity. Overall, the effects of nonlinearity for these cases are consistent with the case of weak EM coupling in Fig. 2(a).

4 Wavepacket Excitation Analysis

To further study the effects of shunt inductance and nonlinearity on system response, the linear and nonlinear chains are excited by a transient wavepacket. Following the similar procedure described in [19], the system is simulated by numerically integrating the governing equations using the built-in MATLAB solver ode89. For these simulations, a semi-infinite metamaterial system is represented by a chain with a large number of cells. Specifically, 500 cells are used to reduce computation time. Pa-

rameters are as detailed in Section 3. The exciting wavepacket is defined by the following set of equations:

$$u_n(0) = \frac{A}{2} \left(H(n-1) - H(n-1 - N_{cy} 2\pi/k) \right)$$

$$\left(1 - \cos(nk/N_{cy}) \right) \sin(nk)$$
(18a)

$$\dot{u}_{n}(0) = \frac{A}{2} \left(H(n-1) - H(n-1-N_{cy}2\pi/k) \right)$$

$$\left(\frac{-\omega}{N_{cy}} sin(nk/N_{cy}) sin(nk) - \omega(1- cos(nk/N_{cy})) \right) cos(nk)$$
(18b)

$$y_n(0) = \Gamma_1 u_n(0) \tag{18c}$$

$$\dot{\mathbf{y}}_n(0) = \Gamma_1 \dot{\mathbf{u}}_n(0) \tag{18d}$$

$$v_n(0) = \Gamma_1 \Gamma_2 u_n(0) \tag{18e}$$

$$\dot{v}_n(0) = \Gamma_1 \Gamma_2 \dot{u}_n(0) \tag{18f}$$

where *n* is the cell number, H() is the Heaviside function, and N_{cy} is the number of cycles, set as $N_{cy} = 7$.

First, the system is simulated for 1500 seconds (nondimensional time) to allow the wavepacket to propagate through the chain. After this period, the spatial profile of the chain's voltage response is studied to examine the effects of nonlinearity. The system is excited within all three modes, and multiple wavenumber regions. Both the default parameter case and the increased inductance case are examined. Selected voltage response profiles for linear and nonlinear chains are shown in Figs. 3-5, with the input (initial excitation) also included for reference. All voltage values are normalized to the peak input voltage.

Fig. 3 shows the response of chains excited within the first mode. Here, the system is excited in the long wavelength region $(k = \pi/9)$; as well as the medium wavelength region $(k = \pi/3)$, where the mode approaches the band gap. In the long wavelength region, Fig. 3(a) and (b), both cases show similar results, with effects of hardening and softening nonlinearity visible but not significant. This small effect of nonlinearity is consistent with the band structure shown in Fig. 2. All values of inductance and nonlinearity show vibration attenuation, with the output voltage profiles an order of magnitude less than the input. In the medium wavelength region, the voltage response is significantly reduced for both cases, indicating that vibration attenuation increases as the band gap is approached. Again, effects of nonlinearity are visible, but not significant. Comparing Fig. 3(c) and (d), the case of increased inductance shows higher voltage amplitude, approximately double of the default case. However, both are two orders of magnitude smaller than the input. When compared to the

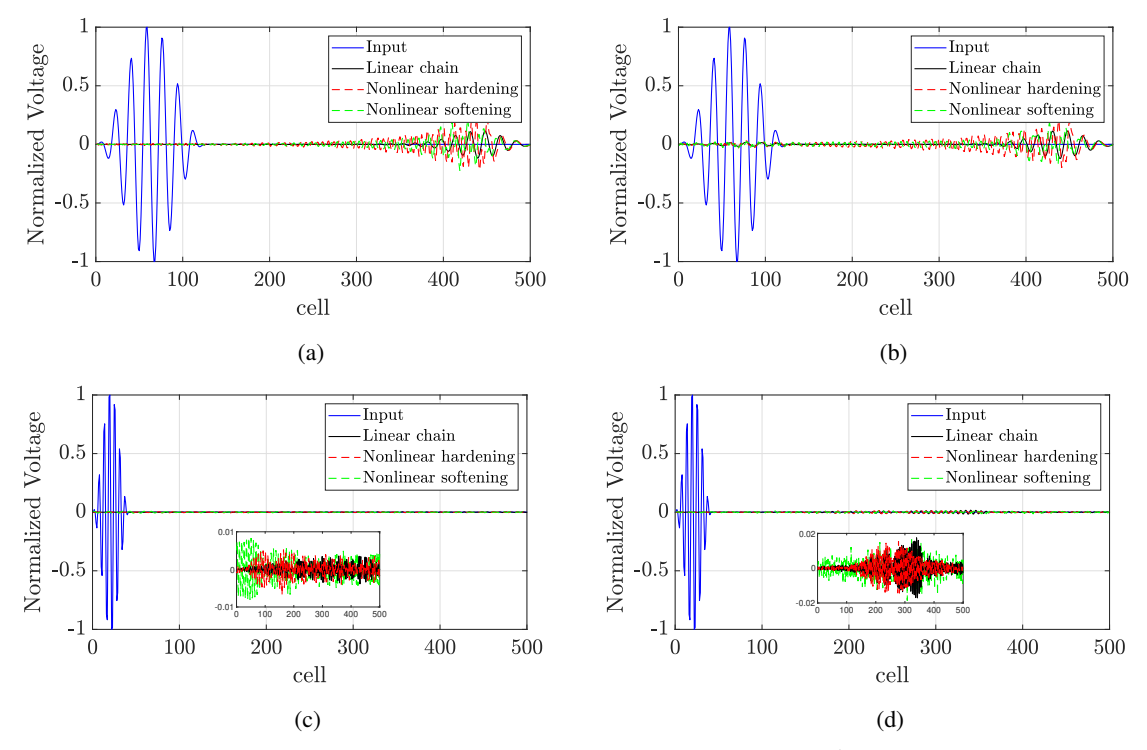


FIGURE 3: Spatial profile of voltage response, first mode branch, for $ω_e = ω_n$, $θ = 10^{-1} N/V$, $m_p/M = 0.1$, $R = 10^3 Ω$: (a) $L = L_0$, k = π/9; (b) $L = 2L_0$, k = π/9; (c) $L = L_0$, k = π/3; (d) $L = 2L_0$, k = π/3.

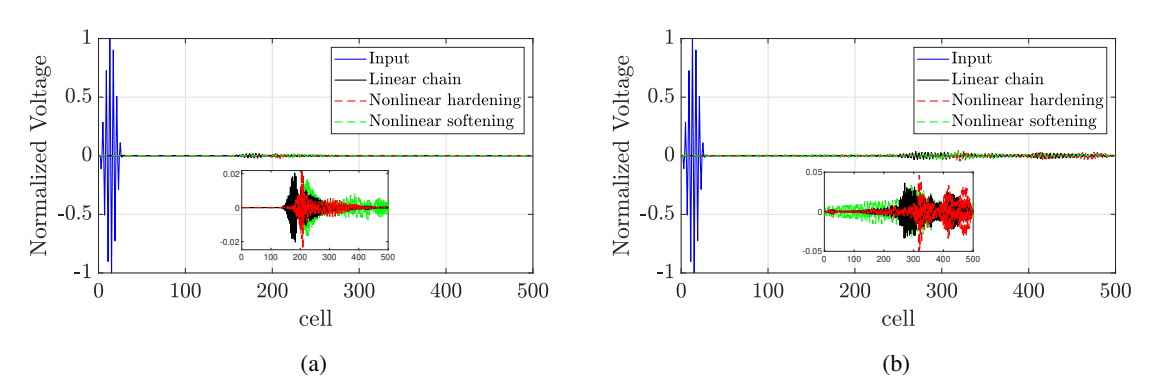


FIGURE 4: Spatial profile of voltage response, second mode branch, for $\omega_e = \omega_n$, $\theta = 10^{-1} \ N/V$, $m_p/M = 0.1$, $R = 10^3 \ \Omega$: (a) $L = L_0$, $k = \pi/2$; (b) $L = 2L_0$, $k = \pi/2$.

corresponding response of the metamaterial with resistance-only shunt studied by Bukhari, there is a clear difference in the effects of nonlinearity [19]. With resistance-only shunt, there is negligible effect of nonlinearity in the long wavelength region, but significant effects in the medium and short wavelength regions, as opposed to the low effects in all regions for the current system. In addition, the resistance-only system does not show the sharp decrease of vibration propagation as the band gap is approached. As shown in Section 3, the presence of inductor introduces an additional band gap, splitting the dispersion curves into three

branches. The resistance-only system includes one less band gap, merging the dispersion curves back into two modes. However, in the inductor system, exciting within the second mode branch can lead to vibration attenuation.

The response of the second mode is shown in Fig. 4. For this mode, only the medium wavelength region $(k = \pi/2)$ is examined. The long and short wavelength regions both show strong vibration attenuation and low effects of nonlinearity consistent with the observations made for the first mode in Fig. 3(c) and (d). At $k = \pi/2$, both the default and increased inductance cases

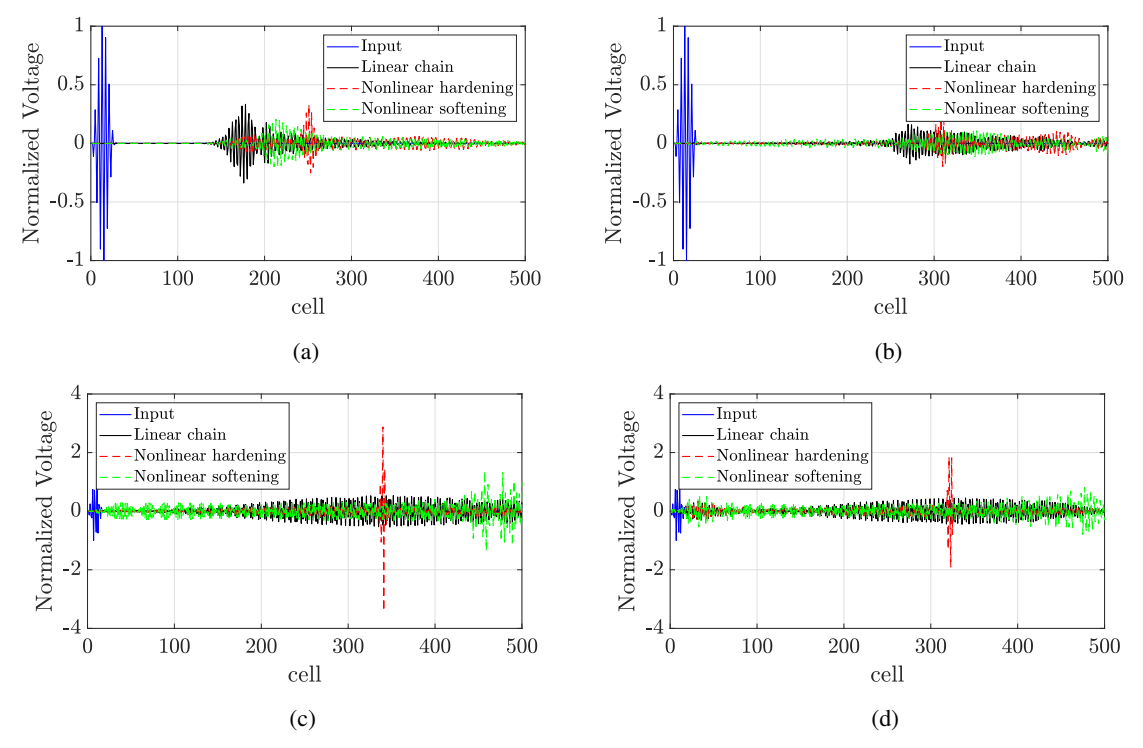


FIGURE 5: Spatial profile of voltage response, third mode branch, for $\omega_e = \omega_n$, $\theta = 10^{-1} \ N/V$, $m_p/M = 0.1$, $R = 10^3 \ \Omega$: (a) $L = L_0$, $k = \pi/2$; (b) $L = 2L_0$, $k = \pi/2$; (c) $L = L_0$, $k = 7\pi/9$; (d) $L = 2L_0$, $k = 7\pi/9$.

have output two orders of magnitude less than the input. Since the medium wavelength region is not near either edge of the pass band, the low wave propagation is not an example of increased attenuation near the band gaps. It can be concluded that the pass band of the second mode branch has very low vibration amplitude in the propagating signal. As in the medium wavelength region of the first mode, the increased inductance case has greater output magnitude, double the output of the default case. Despite the low amplitude, this mode shows significant effects of nonlinearity for both cases. The wave profile of the chain with nonlinear hardening shows the presence of narrow solitary waves, more localized than the linear response and with slightly greater amplitude. The softening chain response is more dispersive than the linear and hardening chains, with a lower amplitude spread out across more of the chain. Overall, in the medium wavelength region, effects of nonlinearity are similar to those observed for the second mode in the resistance-only system [19]. However, the response of the resistance-only system was much larger, matching or exceeding the input amplitude. In addition, the resistance-only system showed larger effects of nonlinearity in the short wavelength region $(k = 7\pi/9)$, in contrast to the small effects in the current case.

In Fig. 5, spatial profiles of the response to excitation within the third mode are shown. The response in the long wavelength

region $(k = \pi/9)$ is not included, but shows low amplitude and effects of nonlinearity near the lower bound of the pass band, similar to Fig. 3(c) and (d). Fig. 5(a) and (b) show the response of the two cases to excitation in the medium wavelength region. Output amplitude is larger than the second mode, though still not as large as the input. The increased inductance case shows slightly smaller output. Effects of nonlinearity are similar to the medium wavelength region of the second mode, with hardening resulting in higher-amplitude solitary waves and softening resulting in lower-amplitude dispersive components. In the short wavelength region ($k = 7\pi/9$), the output amplitude increases, with even the linear and softening responses having amplitude similar to the input. In both cases, the hardening chain response contains a solitary wave with amplitude larger than the input. Again, the increased inductance case has smaller output than the default parameter case. It should be noted that the previously described vibration attenuation near the band gaps is not present at the upper bound of the third mode. Thus, it becomes clear that this attenuation is present near the band gaps between the modes; i.e., the band gaps resulting from the presence of the shunt inductor. Combined with the previously described vibration attenuation across the second mode, this results in a large range with either band gaps or very low wave propagation, an observation with great potential for vibration control. The wave profiles in the third mode are most similar to the response of the second mode in the resistance-only system [19]. While the medium wavelength region still shows smaller response amplitude compared to the resistance-only system, the response in the short wavelength region includes solitary waves with even larger amplitude than the corresponding ones in the resistance-only system.

5 Conclusions

This work contains the analysis of a nonlinear, electromechanical metamaterial coupled to a shunt circuit with both resistor and inductor. The system consists of a chain of cells connected by nonlinear springs, with each cell coupled to an electromechanical resonator consisting of a piezoelectric element and shunt circuit. Both the cells and resonators are modeled as spring-mass systems, with the resonator system also coupled to the dynamics of the shunt circuit. Analytical solutions are used to examine the system's band structure, showing that the effects of adding an inductor to the coupled shunt circuit are only significant for certain parameter values. EM coupling must be strong, $\theta > 10^{-2} N/V$, and shunt resistance must be relatively small, $R < 10^3 \Omega$. For weak coupling or high resistance, the system will behave as a metamaterial with resistance-only shunt. For high coupling and low resistance, the band structure will gain an additional band gap, resulting in a system with three mode branches rather than two.

The behavior of the new band structure is examined through numerical simulation of the metamaterial chain when excited by a transient wave packet. Spatial profiles of the voltage response are provided for multiple values of shunt inductance, illustrating the effects of the added inductor and comparing against a similar system with resistance-only shunt. Several differences are described, including vibration attenuation across the second mode as well as the nearby regions of the first and third modes. The attenuation zones show much less wave propagation that other regions of the first and third modes, and may even be considered band gaps for some purposes. Including the two band gaps resulting from the presence of shunt inductor, this leads to a large attenuation band for vibration control. Furthermore, the effects of changing inductance are shown. Increasing inductance is shown to slightly increase the voltage response in the first two modes, while decreasing amplitude in the third mode. The effects of nonlinearity are also found to differ from the resistance-only system. For the first and second modes, effects of nonlinearity are overall low, though more prominent in the medium wavelength region. The response of the third mode shows prominent effects of nonlinearity, similar to the second mode of the resistance-only system. In the short wavelength region, the voltage response for hardening chain includes solitary waves with amplitudes greater than the corresponding response in the resistance-only system. Overall, the system with inductor provides strong vibration attenuation in a larger frequency range than the corresponding resistor-only system, while increasing output voltage for energy harvesting in other regions. These results for a metamaterial with resistance-inductance shunt set it apart from previously studied systems, and provide multiple options for future exploration of the system and its applications to vibration control and energy harvesting.

6 Acknowledgements

This work is supported in part by the National Science Foundation (NSF) and the NSF CMMI-2038187.

REFERENCES

- [1] Hussein, M. I., Leamy, M. J., and Ruzzene, M., 2014. "Dynamics of phononic materials and structures: Historical origins, recent progress, and future outlook". *Applied Mechanics Reviews*, **66**(4), p. 040802.
- [2] Sigalas, M. M., and Economou, E. N., 1993. "Band structure of elastic waves in two dimensional systems". *Solid state communications*, **86**(3), pp. 141–143.
- [3] Kushwaha, M. S., 1996. "Classical band structure of periodic elastic composites". *International Journal of Modern Physics B*, 10(09), pp. 977–1094.
- [4] Vasseur, J., Djafari-Rouhani, B., Dobrzynski, L., Kushwaha, M., and Halevi, P., 1994. "Complete acoustic band gaps in periodic fibre reinforced composite materials: the carbon/epoxy composite and some metallic systems". *Journal of Physics: Condensed Matter*, **6**(42), p. 8759.
- [5] Liu, Z., Zhang, X., Mao, Y., Zhu, Y., Yang, Z., Chan, C. T., and Sheng, P., 2000. "Locally resonant sonic materials". *science*, 289(5485), pp. 1734–1736.
- [6] Huang, G., and Sun, C., 2010. "Band gaps in a multiresonator acoustic metamaterial". *Journal of Vibration and Acoustics*, 132(3), p. 031003.
- [7] Zhu, R., Liu, X., Hu, G., Sun, C., and Huang, G., 2014. "A chiral elastic metamaterial beam for broadband vibration suppression". *Journal of Sound and Vibration*, 333(10), pp. 2759–2773.
- [8] Bailey, T., and J. Hubbard, J., 1985. "Distributed piezoelectric-polymer active vibration control of a cantilever beam". *Journal of Guidance, Control, and Dynamics*, 8(5), p. 605–611.
- [9] Hagood, N. W., and von Flotow, A., 1991. "Damping of structural vibrations with piezoelectric materials and passive electrical networks". *Journal of Sound and Vibration*, **146**(2), p. 242–268.
- [10] Dosch, J. J., Inman, D. J., and Garcia, E., 1992. "A self-sensing piezoelectric actuator for collocated control". *Journal of Intelligent Material Systems and Structures*, 3(1), p. 166–185.

- [11] Arafa, M., and Baz, A., 2000. "Dynamics of active piezoelectric damping composites". *Composites Part B: Engineering*, 31(4), p. 255–264.
- [12] Thorp, O., Ruzzene, M., and Baz, A., 2001. "Attenuation and localization of wave propagation in rods with periodic shunted piezoelectric patches". *Smart Materials and Structures*, *10*(5), p. 979.
- [13] Airoldi, L., and Ruzzene, M., 2011. "Wave propagation control in beams through periodic multi-branch shunts". *Journal of Intelligent Material Systems and Structures*, 22(14), pp. 1567–1579.
- [14] Casadei, F., Delpero, T., Bergamini, A., Ermanni, P., and Ruzzene, M., 2012. "Piezoelectric resonator arrays for tunable acoustic waveguides and metamaterials". *Journal of Applied Physics*, 112(6), p. 064902.
- [15] Beck, B. S., Cunefare, K. A., Ruzzene, M., and Collet, M., 2011. "Experimental analysis of a cantilever beam with a shunted piezoelectric periodic array". *Journal of Intelligent Material Systems and Structures*, 22, p. 1177–1187.
- [16] Wang, G., and Chen, S., 2015. "Large low-frequency vibration attenuation induced by arrays of piezoelectric patches shunted with amplifier-resonator feedback circuits". *Smart Materials and Structures*, **25**, p. 331–346.
- [17] Sugino, C., Leadenham, S., and Ruzzene, M., 2017. "An investigation of electroelastic bandgap formation in locally resonant piezoelectric metastructures". *Smart Materials and Structures*, **26**, 05, p. 055029.
- [18] Erturk, A., and Inman, D. J., 2011. *Piezoelectric energy harvesting*. John Wiley & Sons.
- [19] Bukhari, M. A., and Barry, O., 2020. "Simultaneous energy harvesting and vibration control in a nonlinear metastructure: A spectro-spatial analysis". *Journal of Sound and Vibration*, 473, p. 115215.
- [20] Abdelmoula, H., and Abdelkefi, A., 2015. "Ultra-wide bandwidth improvement of piezoelectric energy harvesters through electrical inductance coupling". *The European Physical Journal Special Topics*, **224**, pp. 2733–2753.
- [21] Nayfeh, A. H., 2011. *Introduction to perturbation techniques*. John Wiley & Sons.